Persisting α-planar structure in ^{20}Ne

P. K. Kakanis
Greek Atomic Energy Commission, Aghia Paraskevi-Attiki, 153 10 Greece

G. S. Anagnostatos
Department of Physics, University of Oxford, Nuclear Physics Laboratory, Keble Road, Oxford, OX1 3RH, United Kingdom and Institute of Nuclear Physics, National Center for Scientific Research ''Demokritos,'' Aghia Paraskevi-Attiki, 153 10 Greece

(Received 23 May 1996)

Nine low-lying O_n^+ states of ^{20}Ne and their possible rotational bands have been studied by employing the isomorphic shell model which is a hybrid between conventional shell model and the liquid drop model in conjunction with the nucleon finite size and which in addition uses no adjustable parameters. The configurations of six out of these nine O_n^+ states have an α-planar structure when, for each set of four closeby nucleon average positions (two protons and two neutrons), possessing the same principal quantum number n and forming an instant α-like particle, the center of gravity is considered. The novelty of the present study is focused on the fact that the axis of rotation and the number of rotating nucleons inside the same rotational band may change in such a way that the relevant moment of inertia increases monotonically in steps forming for each step a new branch of the band. Up to five such branches have been found and each time the moment of inertia of the last of them approaches the rigid body limit, creating superdeformed bands. The coexistence of a superdeformed band and of lower deformation bands include several states with the same I^π value. Two rotational bands are introduced for the first time and the model predictions of states in all cases are very close to the experimental data. Another important feature of the present study is that two different configurations possess identical binding energy (the maximum among all possible configurations) and are assigned, by 50% each, to the g.s. of ^{20}Ne. This has been verified by successfully employing many observables and results of other models. [S0556-2813(96)05612-9]

PACS number(s): 21.60.Gx, 21.10.Re, 27.30.+t

I. INTRODUCTION

The nucleus ^{20}Ne lies in the middle of the $A=4n$ (where $n=1-0$) nuclei, i.e., between the two doubly closed-shell nuclei ^{4}He and ^{40}Ca. This location makes the spectrum of ^{20}N rich, i.e., it possesses a large number of low-lying levels. Of particular importance are the many low lying O^+ levels which constitute the subject of many publications which use several models for their interpretation. The study of these levels and particularly of those which are band heads of rotational spectra [1–5] constitutes a very sensitive test for the different models employed. These and their rotational bands, together with other observables of ^{20}Ne, are the subject matter of the present work which employs the semiclassical [6] part of the isomorphic shell model. The semiclassical instead of the quantum-mechanical [7] part of the model is utilized since it provides a pictorial approach easily compared with that of the α-cluster models [8–31] which are among the models frequently used in the investigation of $4n$ nuclei. Indeed, studies of light nuclei in general and of ^{20}Ne in particular indicate the important role of α clustering in these nuclei.

The literature lists [2] many empirical rotational bands for ^{20}Ne. Although doubt has been expressed as to whether these empirical bands correspond to any real rotational motion [5], theoretical calculations in the framework of both the shell model and the cluster models have had relatively good success in accounting for many of the band characteristics [1]. Among the different studies, that of Ref. [1] (based on reduced widths for α decay to the ground state of ^{16}O) constitutes the most thorough and critical one concerning the judgement of previous assignments of states to the different bands in ^{20}Ne and stands as the basic reference of the present work.

The ability of the isomorphic shell model to estimate the moments of inertia without the knowledge of experimental rotational data being necessary warrants a reexamination of previous assignments and the recommendation of new ones for rotational bands in ^{20}Ne. Furthermore the model which considers the interaction of each individual nucleon with all other nucleons in a nucleus, through the present application, may provide a lot of information about the intrinsic nuclear structure in general, and may contribute towards the microscopic explanation of nuclear properties including excitation mechanisms in particular, subjects which are among the most important aims in the nuclear many-body problem.

This work on ^{20}Ne parallels our previous work on ^{12}C [30] and on ^{28}Si [31], employing the same model.

II. THE ISOMORPHIC SHELL MODEL

The model includes both a fully quantum-mechanical [7] part and a semiclassical [6] part and has been presented in many previous publications (see references in [30,31]). Perhaps the most concise presentation of the model is that included in Ref. [30]. Since the model is still relative;ly new, however, many readers could expect applications of the model, as the present one, to be accomplished by a brief review of the model. Here, in order to avoid repetitions from previous publications, only the main concepts are reviewed

together with the technical part of the model referring to the formulas necessary for the present work to become self-sufficient.

A. Main features of the model

The quantum-mechanical part is fully developed in Ref. [7a], where, for the first time, nuclear binding energies and radii are simultaneously reproduced in good agreement with the experimental data. Further development of this part of the model is represented in Ref. [7b], where the model reproduces successfully the high components of proton momentum distribution in nuclei beyond Helium-4. The semiclassical part is the one here applied since it is closer to the α-cluster model and thus a comparison between them is easier and more comprehensive. The relationship between the quantum-mechanical part and the semiclassical part of the model will become apparent shortly. The next section pertains to all formulas necessary for its present implementation.

The isomorphic shell model is a microscopic nuclear-structure model that incorporates into a hybrid model the prominent features of single-particle and collective approaches in conjunction with the nucleon finite size [6,7].

The single-particle component of the model is along the lines of the conventional shell model with the only difference that in the model the nucleons creating the central potential are the nucleons of each particular nuclear shell alone, instead of all nucleons in the nucleus as assumed in the conventional shell model [7a]. In other words, we consider a multiharmonic potential description of the nucleus (as many potentials as shells), as follows:

$$H\Psi = E\Psi, \quad H = T + V, \tag{1}$$

$$H = H_{1s} + H_{1p} + H_{1d2s} + \cdots, \tag{2}$$

where

$$H_i = V_i + T_i = \overline{V} + \tfrac{1}{2} m(\omega_i)^2 r^2 + T_i\,. \tag{3}$$

That is, we consider a state-dependent Hamiltonian, where each partial harmonic oscillator potential has its own state-dependent frequency ω_i. All these ω_i's are determined from the harmonic oscillator relation

$$\hbar\omega_i = \frac{\hbar^2}{m\langle r_i^2\rangle}\left(n + \frac{3}{2}\right), \tag{4}$$

where n is the harmonic oscillator quantum number and $\langle r_i^2\rangle^{1/2}$ is the average radius of the relevant high fluximal shell determined by the semiclassical part of the model specified below. For details on $\overline{V}$ one should consult Ref. [7a].

The solution of the Schrödinger equation with Hamiltonian (2), in spherical coordinates, is

$$\Psi_{nlm}(r,\theta,\phi) = R_{nl}(r) Y_l^m(\theta,\phi), \tag{5}$$

where $Y_l^m(\theta,\phi)$ are the familiar spherical harmonics and the expressions for the $R_{nl}(r)$ are given in several books of quantum mechanics and nuclear physics.

The only difference between our wave functions and those in these books is the different ω's as stated in Eqs. (3) and (4) above. Those of our wave functions, however, which have equal l value, because of the different $\hbar\omega$, are not orthogonal, since in these cases the orthogonality of Legendre polynomials does not suffice. Orthogonality, of course, can be obtained by applying established procedures, e.g., the Gram-Schmidt process [7b].

According to Hamiltonian (2), the binding energy of a nucleus with A nucleons in the case of orthogonal wave functions takes the simple form given by Eq. (6)

$$E_B = 1/2(\overline{V}\cdot N) - 3/4\left[\sum_{i=1}^{A} \hbar\omega_i(n+3/2)\right], \tag{6}$$

where $\overline{V}$ is the average potential depth. The coefficients 1/2 and 3/4 take care of the double counting of nucleon pairs in determining the potential energy.

Applications and details of the quantum-mechanical part of the model are given in Refs. [7a] and [7b]. Here an application of the semiclassical part [6,30] in the place of the quantum-mechanical part of the model is considered in the spirit of the Ehrenfest's theorem [30], which for the observables of position ($\vec{R}$) and momentum ($\vec{P}$) takes the form

$$\frac{d}{dt}\langle\vec{R}\rangle = \frac{1}{m}\langle\vec{P}\rangle \tag{7}$$

and

$$\frac{d}{dt}\langle\vec{P}\rangle = -\langle\nabla V(\vec{R})\rangle \tag{8}$$

The quantity $\langle\vec{R}\rangle$ represents a set of three time-dependent numbers $\{\langle X\rangle, \langle Y\rangle, \langle Z\rangle\}$ and the point $\langle\vec{R}\rangle(t)$ is the center of the wave function at the instant t. The set of those points which corresponds to the various values of t constitutes the trajectory followed by the center of the wave function.

From Eqs. (7) and (8) we get

$$m\frac{d^2}{dt^2}\langle\vec{R}\rangle = -\langle\nabla V(\vec{R})\rangle. \tag{9}$$

Furthermore, it is known that, for the special case of the harmonic oscillator potential assumed by the isomorphic shell model in Eq. (3), the following relationship is valid

$$\langle\nabla V(\vec{R})\rangle = [\nabla V(\vec{r})]_{\vec{r}=\langle\vec{R}\rangle}, \tag{10}$$

where

$$[-\nabla V(\vec{r})]_{\vec{r}=\langle\vec{R}\rangle} = \vec{F}. \tag{11}$$

That is, for this potential the average of the force over the whole wave function is rigorously equal to the classical force F at the point where the center of the wave function is situated. Thus, for the special case (harmonic oscillator) considered, the motion of the center of the wave function obeys the laws of classical mechanics. Any difference between the quantum and the classical description of the nucleon motion depends exclusively on the degree the wave function may be approximated by its center. Such differences will contribute

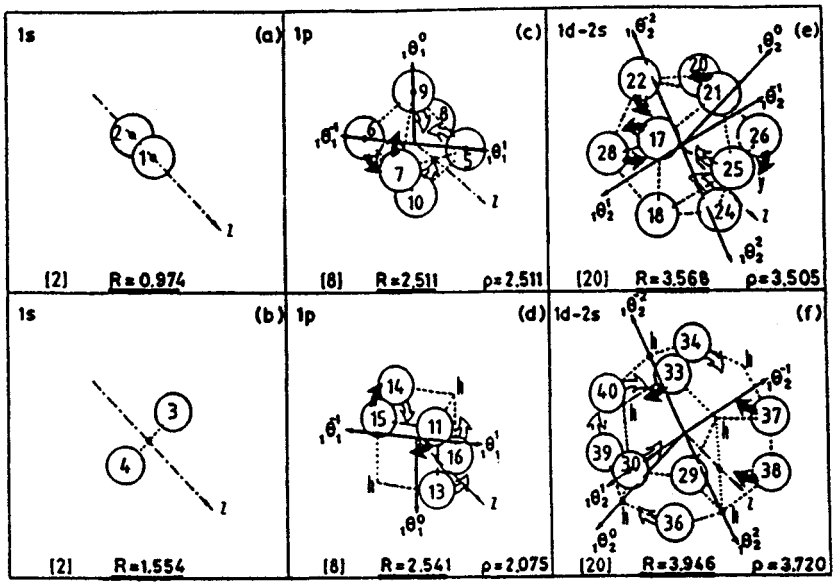

FIG. 1. The isomorphic shell model for the nuclei up to $N=20$ and $Z=20$. The high-symmetry polyhedra in row 1 (i.e., the zerohedron, the octahedron, and the icosahedron) stand for the average forms for neutrons if (a) the $1s$, (c) the $1p$, and (e) the $1d2s$ shells, while the high-symmetry polyhedra in row 2 [i.e., the zerohedron, the hexahedron (cube), and the dodecahedron] stand for the average forms of (b) the $1s$ (d) the $1p$, and (f) the $1d2s$ shells for protons. The vertices of polyhedra stand for the average positions of nucleons in definite quantum states (τ,n,l,m,s). The letters h stand for the empty vertices (holes). The z axis is common for all polyhedra when these are superimposed with a common center and with relative orientations as shown. At the bottom of each block the radius R of the sphere exscribed to the relevant polyhedron and the radius ρ of the relevant classical orbit, equal to the maximum distance of the vertex state (r,n,l,m,s) from the axis ${}_n\theta_l^m$ representing precisely the orbital angular-momentum axis with definite n, l, and m values, are given. Curved arrows shown help the reader to visualize which axis each nucleon rotates round, while solid (open) arrows show rotations directed up (down) the plane of the paper. All polyhedra vertices are numbered as shown. The backside (hidden) vertices of the polyhedra and the related numbers are not shown in the figure.

to the magnitude of deviations between the experimental data and the predictions of the semiclassical part of the model employed here.

Now, in the semiclassical treatment the nuclear problem is reduced into that of studying the centers of the wave functions presenting the constituent nucleons or, in other words, of studying the average positions of these nucleons. For this study the following two assumptions are employed by the isomorphic shell model.

(i) The neutrons (protons) of a closed neutron (proton) shell, considered at their *average* positions, are in *dynamic equilibrium* on the sphere presenting the average size of that shell.

(ii) The average sizes of the shells are determined by the *close-packing* of the shells themselves, provided that a neutron and a proton are represented by *hard spheres* of definite sizes (i.e., $r_n=0.974$ fm and $r_p=0.860$ fm).

It is apparent that assumption (i) is along the lines of the conventional shell model, while assumption (ii) is along the lines of the liquid-drop model.

The model employs a specific equilibrium of nucleons, considered at their average positions on concentric spherical cells, which is valid whatever the law of nuclear force may be: assumption (i). This equilibrium leads uniquely to Leech [32] (equilibrium) polyhedra as average forms of nuclear shells. All such nested polyhedra are closed packed, thus, taking their minimum size: assumption (ii). The cumulative number of vertices of these polyhedra, counted successively from the innermost to the outermost, reproduces the magic numbers each time a polyhedral shell is completed [6] (see the numbers in the brackets in Fig. 1 there).

For one to conceptualize the isomorphic shell model, he should first relate this model to the conventional shell model. Specifically, the main assumption of the simple shell model, i.e., that each nucleon in a nucleus moves (in an average potential due to all nucleons) independently of the motion of the other nucleons, may be understood here in terms of a *dynamic equilibrium* in the following sense [6]. Each nucleon in a nucleus is *on average* in a *dynamic equilibrium* with the other nucleons and, as a *consequence*, its notion may be described independently of the motions of the other nucleons. From this one realizes that dynamic equilibrium and independent particle motion are *consistent* concepts in the framework of the isomorphic shell model.

In other words, the model implies that *at some instant in time* (reached *periodically*) all nucleons could be thought of as residing at their individual average positions, which coincide with the vertices of an equilibrium polyhedron for each shell. This system of particles evolves in time according to each independent particle motion. This is possible, since axes standing for the angular momenta quantization of directions are *identically* described by the rotational symmetries of the polyhedra employed [33–36]. For example, see Ref. [35], where one can find a complete interpretation of the independent particle model in relation to the symmetries of these polyhedra. Such vectors are shown in Fig. 1 for the orbital angular-momentum quantization of directions involved for nuclei up to $N=20$ and $Z=20$.

Since the radial and angular parts of the polyhedral shells in Fig. 1 are well defined, the coordinates of the polyhedral vertices (nucleon average positions) can be computed easily. These coordinates up to $N=Z=20$ are already published in footnote 14 of Ref. [37], and in Refs. [38,39]. These coordinates correspond to the R values of the exscribed polyhedral spheres given in Fig. 1 (see bottom line at each block).

According to the isomorphic shell model, the nucleon average positions of a nucleus are distributed at the vertices of the polyhedral shells as shown, for example, in Fig. 1. The specific vertices occupied, for a given (closed- or open-shell) nucleus at the ground state, form a vertex configuration (corresponding to a state configuration) that possesses the maximum binding energy (E_B) in relation to any other possible vertex configuration which, thus, stands for an excited state. Each vertex configuration defines the average form and structure of a relevant state of this nucleus. All bulk (static) properties of this state (e.g., E_B, rms radii, etc.) are derived as properties of this structure, as has been fully explained in Ref. [6] and references cited therein.

B. Technical features of the model

The model employs a two body potential in the form of two Yukawa functions [37]:

$$V_{ij}=1.7(10^{17})\frac{e^{-(31.8538)r_{ij}}}{r_{ij}}-187\frac{e^{-(1.3538)r_{ij}}}{r_{ij}} \quad \text{(in MeV)}, \tag{12}$$

where the internucleon distance r_{ij} between average positions i and j are estimated by using the relevant coordinates.

The Coulomb potential between two proton average positions apparently is:

$$(E_C)_{ij}=\frac{e^2}{r_{ij}} \tag{13}$$

where r_{ij} as has been defined above.

The average kinetic energy for each nucleon is taken as the sum of the kinetic energy due to the uncertainty principle and of the kinetic energy due to the orbiting of the nucleon [38]:

$$\langle T\rangle_{nlm}=\frac{\hbar^2}{2M}\left[\frac{1}{R_{\max}^2}+\frac{1(1+1)}{\rho_{nlm}^2}\right], \tag{14}$$

where $R_{\max}$ is the outermost polyhedral radius R plus the relevant average nucleon radius (i.e., $r_n=0.974$ fm or $r_p=0.860$ fm), i.e., the radius of the nuclear volume in which the nucleons are confined, M is the nucleon mass, ρ_{nlm} is the distance of the vertex (n,l,m) from the axis ${}_n\theta_l^m$ (see Fig. 1 and Refs. [33–36,38])

The spin-orbit interaction in the model is given below [40]:

$$(E_{\mathrm{SO}})_i=-(20\pm5)A^{-2/3}\boldsymbol{l}_{\mathbf{i}}\cdot\mathbf{s}_{\mathbf{i}} \tag{15}$$

The energy coefficient ($20\pm5=15$–25 MeV) starts at its lower values for the lower orbital angular momenta and tends more or less smoothly to the larger values for the higher orbital angular momenta. As also is known, for $j=1+1/2$, $\boldsymbol{l}\cdot\boldsymbol{s}=+1/2$, while for $j=1-1/2$, $\boldsymbol{l}\cdot\boldsymbol{s}=-(1+1)/2$.

The collective rotational energy is given by Eq. (16)

$$E_{\mathrm{rot}}=\frac{\hbar^2 I(I+1)}{2J}, \tag{16}$$

where **J** is the moment of inertia of the rotating part of the nucleus given by Eq. (17)

$$J=\sum_i^{N_{\mathrm{rot}}} m\rho_i^2=mN_{\mathrm{rot}}\langle r^2\rangle_{\mathrm{rot}}, \tag{17}$$

where N_{rot} is the number of nucleons participating in the collective rotation and $\langle r^2\rangle_{\mathrm{rot}}$ is the mean square radius of these nucleons. This value of J is increased by the quantity $(0.165)N_{\mathrm{rot}}$, where the coefficient stands for the contribution to the moment of inertia coming from the finite size of each nucleon participating in the rotation [30].

The binding energy in the model, now, is

$$E_B=-\sum_{\substack{\text{all nucleon}\\ \text{pairs}}} V_{ij}-\sum_{\substack{\text{all proton}\\ \text{pairs}}}\frac{e^2}{r_{ij}}-\sum_{\text{all nucleons}}\langle T\rangle_{nlm}+\sum_{\substack{\text{all valence}\\ \text{nucleons}}} E_{(\mathrm{SO})i}, \tag{18}$$

where the terms E_δ (odd-even) and E_{rot} (collective rotation) appearing in Eq. (15) of Ref. [30] for the binding energy are omitted here as irrelevant to the case of interest, i.e., ^{20}Ne.

The rms charge radius is given by Eq. (19)

$$\langle r^2\rangle_{\mathrm{ch}}^{1/2}=\left[\frac{\Sigma_{i=1}^{Z}R_i^2}{Z}+(0.8)^2-(0.116)\frac{N}{Z}\right]^{1/2}, \tag{19}$$

where R_i is the radius of the ith proton average position from Fig. 1, Z and N are the proton and the neutron numbers of the nucleus, and $(0.8)^2$ and (0.116) are the mean square charge radii of a proton and of a neutron, respectively [41].

The intrinsic electric quadrupole moment is given by Eq. (20)

$$eQ'_{20}=\sum_i eQ'_{(20)i}=\sum_{i=1}^{Z} eR_i^2(3\cos^2\theta_i-1), \tag{20}$$

where R is the radius of the ith proton average position and θ_i is the corresponding azimuthal angle with respect to the symmetry axis [42].

The intrinsic electric octupole moment is given by Eq. (21):

$$eQ'_{30}=\sum_i eQ'_{(30)i}=\sum_{i=1}^{Z} eR_i^3(5\cos^2\theta_i-3)\cos\theta_i. \tag{21}$$

The intrinsic electric hexadecapole moment is given by Eq. (22):

$$eQ'_{40}=\sum_i eQ'_{(40)i}=\sum_{i=1}^{Z} eR_i^4(35\cos^4\theta_i-30\cos^2\theta_i+3), \tag{22}$$

where R_i and θ_i as for Q'_{20} and Q'_{30} above [43,44].

The reduced electric-quadrupole transition probability between the 0^+ ground state and the first 2^+ state in even-even nuclei which exhibit a rotational [42] spectrum is given by Eq. (23):

$$B_{(E2)_{\rm ex}}({\rm cm}^4) = 4.08\times 10^{-61}[E_\gamma({\rm MeV})]^{-5}[\tau({\rm sec})]^{-1} \times[1+\alpha_T]^{-1} = Q_0^2 5/(16\pi) = \beta_2^2[3ZR_o^2/4\pi]^2, \quad (23)$$

where E_γ and τ are the excitation energy and the mean life of the first 2^+ state, α_T is the internal conversion coefficient, and β_2 is the deformation parameter which for a spheroid nucleus with semimajor and semiminor axes a and b takes the expression [42]

$$\beta_2 = 1.06(a-b)/R_0, \quad (24)$$

where $R_0 = r_0 A^{1/3}$ is the nuclear average radius.

Equations (12)–(23) stand here for all formulas necessary for the implementation of the semiclassical part of the model.

III. CALCULATIONS

Average structures of ^{20}Ne, in the framework of the isomorphic shell model, come from Fig. 1 by considering the states $1s$, $1p$, and $1d5/2$ involved in this nucleus. Figure 2 shows all possibilities of α-like cluster structures of ^{20}Ne offered by Fig. 1 in accommodating 10 neutron average positions on the neutron polyhedra (first row of Fig. 1) and 10 proton average positions on the proton polyhedra (second row of Fig. 1). Specifically, Figs. 2(a)–(c) stand for the average structures of ^{20}Ne possessing a ^{16}O core and one α-like particle on either the x, or y, or z axis, respectively, while Figs. 2(d)–(i) stand for the average structures of ^{20}Ne possessing a ^{12}C core and two α-like particles on the axes x, y, and z, that it, either two α-like particles on the x axis [Fig. 2(d)], or on the y axis [Fig. 2(e)], or on the z axis [Fig. 2(f)], or the one α-like particle on the x axis and the other on the y axis [Fig. 2(g)], or on the y axis and on the z axis [Fig. 2(h)], or on the z axis and on the x axis [Fig. 2(i)].

For each part of Figs. 2(d)–(i) two cases are considered. For the first case [first column from (d)–(i)], the $1s1/2$ proton average positions are those numbered 3 and 4 in Figs. 1 and 2, while for the second case [second column from (d)–(i)], the average positions of these two protons are those called ''relaxed,'' i.e., 3_r and 4_r (not shown in Figs. 1 and 2), resulting from rotation of 3 and 4 around the nuclear center in such a way that their bags stay in contact with those of 1 and 2, and in addition come in contact with those of 5,8 and 6,7, respectively. This relaxation leads to larger potential energy and finally to larger binding energy, since the other energy components involved do not have a noticeable variation. The corresponding coordinates are for the average position 3: $x=-0.897$ fm, $y=z=0.897$ fm and for the average position 4: $x=0.897$ fm, $y=z=-0.897$ fm, while for the average position 3_r: $x=-1.006$ fm, $y=1.006$ fm, $z=0.3737$ fm and for the average position 4_r: $x=1.006$ fm, $y=-1.006$ fm, $z=-0.3737$ fm. Similar consideration of 3_r and 4_r, instead of 3 and 4, has been made for ^{12}C [30] and for ^{28}Si [31]. Such a relaxation of 3 and 4 is possible only if the $1p1/2$ neutrons (whose average positions are numbered 9 and 10 in Figs. 1 and 2) are absent from the relevant nuclear structure, e.g., in the cases of ^{12}C core. Finally, while in the test the distinction between 3,4 and 3_r,4_r is made by naming the relevant figure as ''relaxed,'' Figs. 2(d)–(i) is considered to present both cases.

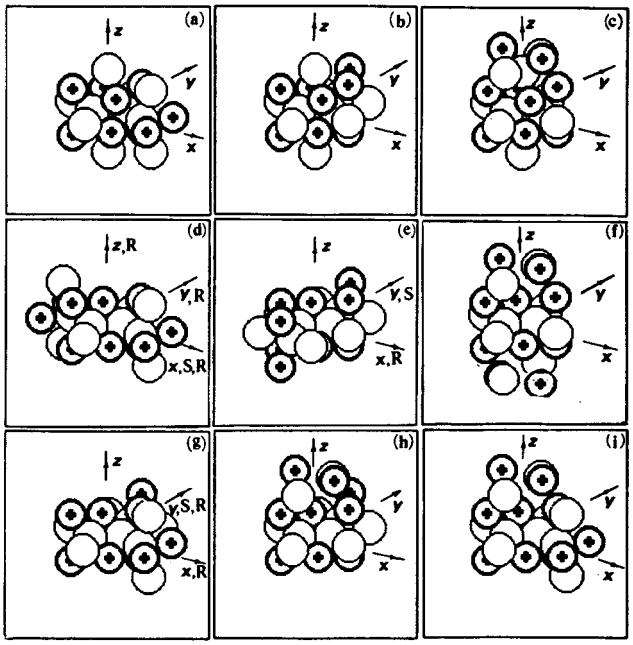

FIG. 2. Average forms of ^{20}Ne, according ot the isomorphic shell model, composed of the average positions of the constituent nucleons (NAP) forming α-like particles. (a) ^{16}O core (NAP 1-16) plus one ''α particle on the x axis (NAP 17-18, 29-30), (b) ^{16}O core plus one ''α'' particle on the y axis (NAP 25-26, 37-38), (c) ^{16}O core plus one ''α'' particle on the z (NAP 21-22, 33-34), (d) ^{12}C core (NAP 1-8, 11-14) plus two ''α'' particles on the x axis (NAP 17-18, 29-30; 19-20; 31-32), (e) ^{12}C core plus two ''α'' particles on the y axis (NAP 25-26, 37-38; 27-28, 39-40), (f) ^{12}C core plus two ''α'' particles on the z axis (NAP 21-22, 33-34, 23-24; 35-36), (g) ^{12}C core plus one ''α'' particle on the x axis and one ''α'' particle on the y axis (NAP 17-18, 29-30; 25-26; 37-38), (h) ^{12}C core plus one ''α'' particle on the y axis and one ''α'' particle on the z axis (NAP 25-26, 37-38, 21-22, 33-34), and (i) ^{12}C core plus one ''α'' particle on the z axis and one ''α'' particle on the x axis (NAP 21-22, 33-34, 17-18, 29-30). Each of the parts (d)–(i) stands for both the ''normal'' and ''relaxed'' average positions of the two $1s$ protons (Nos. 3 and 4). Average nucleon positions are numbered as shown by using for the same positions the same number as in Fig. 1. Axes labelled x,y,z stand for the axes of coordinates and those labelled S and R for symmetry and rotation axes, respectively, as used in the calculations of Secs. III and IV.

The aforementioned difference in the core at the different parts of Fig. 2, i.e., that the parts Figs. 2(a)–(c) have a ^{16}O core, while the parts Figs. 2(d)–(i) have a ^{12}C core, as will become apparent shortly, leads to the fact that the parts (a)–(c) have a three-dimensional structure, while the parts (d)–(i) have a two-dimensional structure in an α-like clusterwise representation. Specifically, in Figs. 2(a)–(c) each set of the following four nucleon average positions numbered (1-2,3-

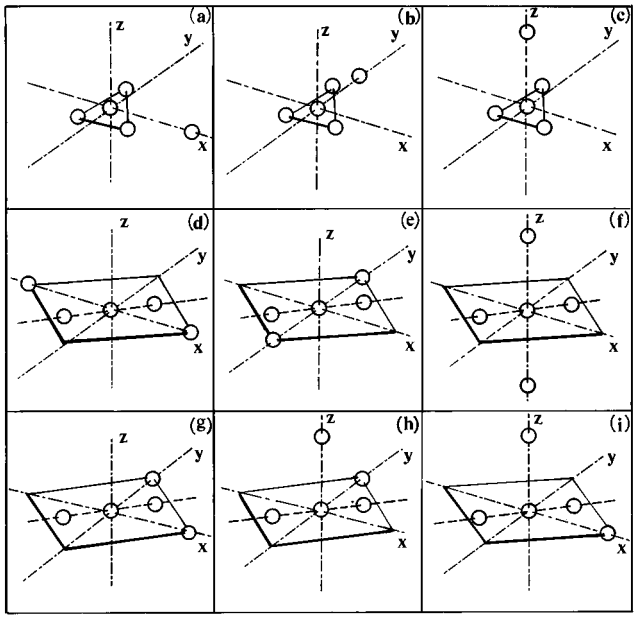

FIG. 3. Average forms of ^{20}Ne, according to the isomorphic shell model, derived from those of Fig. 2 when for each α-like particle its center of gravity is considered. Each part of Fig. 3 has its counterpart in Fig. 2 of the same alphabetic labeling. Thus $1s$ nucleons form an ''α'' particle at the nuclear center, while $1p$ nucleons form ''α'' particles either forming an equilateral triangle [parts (a)–(c)] around the center or forming a straight line with the center [parts (d)–(i)]. Finally, $1d$ nucleons form ''α'' particles at the vertices of a regular octahedron around the center.

4), (5,10,13,16), (6,8,12,14), (7,9,11,15), (17-18, 29-30), (19-20, 31-32), (25-26,37-38), (27-28, 39-40), (21-22, 33-34), and (23-24, 35-36) accommodates two protons and two neutrons with the same n quantum number which are close together for the instant depicted by this figure, while in Figs. 2(d)–(i) the different sets (5,7,11,13) and (6,8,12,14) for the $1p$ nucleons, together with the possibility of the set $(1–2,3_r–4_r)$ instead of the set (1–2, 3–4) for the $1s$ nucleons, should be considered.

Thus, in the model, each of these sets of four nucleons can be taken as an instant α-like particle. Considering now the center of gravity for each of these ''α-particles'' Figs. 3(a)–(i) results. Specifically, in Figs. 3(a)–(c) a central α-like particle is surrounded on the same plane by three α-like particles forming an equilateral triangle, while the last α-like particle lies outside the triangle on one of the axes of coordinates, as noted. In Figs. 3(d), (e), (g) all α-like particles *precisely* lie on the same plane (i.e., their centers are coplanar, either using the pair 3-4 or the pair 3_r-4_r) formed by an interior straight segment and an exterior square (as noted), only two vertices of which are occupied by two α-like particles. In Fig. 2(f) the five α-like particles form a cross. Finally, in Fig. 3(h)–(i) the α-like particles form a three-dimensional structure made of the same interior straight segment and of the last two α-like particles lying on either the y,z or z,x axes of coordinates (as noted). The line segment mentioned above is *identical* to ^{12}C [30] appearing also as a core in ^{28}Si [31], while the square is *identical* to that discussed in ^{28}Si [31].

It is worth noting that the valence α-like particles in all parts of Figs. 3(a)–(i) lie at the vertices of a regular octahedron, only one or two vertices of which (in each part of the figure as noted) are occupied by these α-like particles. All of its vertices, of course, are occupied in ^{40}Ca, where totally three shells of α-like particles are filled, i.e., the one made of one α-like particle at the nuclear center standing for the $1s$ states, the next made of three α-like particles forming an equilateral triangle standing for the $1p$ states, and the last made of six α-like particles forming a regular octahedron standing for the $1d$-$2s$ states.

For moments later than that depicted by all three Figs. 1–3, each of the four nucleons composing any of the above α-like particles evolves by following its own independent particle motion in a well-specified shell model orbital. That is, each nucleon will rotate in a shall model orbital around its own axis of orbital angular momentum labeled in the figure by the proper ${}_n\theta_l^m$ angle with respect to the quantization axis z common for all parts of Fig. 1.

As mentioned early in this section, Fig. 2 shows all possible α-particle like cluster structures of ^{20}Ne in the framework of the isomorphic shell model. Table I is divided into nine blocks arranged in correspondence with those of Figs. 2 and 3. The first listed vertex (state) configuration (sequence of numbers) in each block of the table is that presented in the corresponding block of Figs. 2 and 3. The other configurations listed in the table are the equivalent ones and are not presented in the figures.

By applying Eqs. (1)–(4) the numerical values for each of the four terms (right-hand side) in Eq. (7), for each vertex (state) configuration of Table I (row 2), are listed in rows 3–6 in the same block of the table. The summation of the above four terms gives the net energy E_B, which is listed in row 7 of each block. Comparing the values of this column in all blocks we assign the proper I_n^+ value listed in row 11 of each block together with the predicted excitation energy (row 8), and the corresponding experimental excitation energy (row 9) and level width (row 10). Indeed, configurations (e) relaxed and (g) relaxed have identical binding energy, which is the maximum of the table, and thus they are identified as ground-state configurations and all others as excited configurations. Specifically, the aforementioned g.s. configurations have a binding energy 15.85 MeV above the experimental 160.55 MeV g.s. energy, while the excitation energies (with respect to the g.s.) of all other configurations of Table I are positive as follows: configuration (a) 9.1 MeV (8,8), (b) 8.6 MeV (8.7), (c) 10.3 MeV (10,8), (d) 16.2 MeV (16.4), d relaxed 7.0 MeV (6.7), (e) 13.0 MeV (13.2), (f) 75.9 MeV, (f) relaxed 71.6 MeV, (g) 11.1 MeV (11.0), (h) 40.9 MeV, (h) relaxed 32.2 MeV, (i) 42.5 MeV, and (i) relaxed 35.7 MeV, where inside parentheses the associated experimental energies are given and will be discussed shortly.

For the configurations of Table I with excitation energies above 28.2 MeV, which is the limit up to which the spectrum of ^{20}Ne is known today [2], no comment can be made except that all these fix configurations namely, (f), (f) relaxed, (h), (h) relaxed, (i) and (i) relaxed have $I^\pi=O^+$ and that they contain at least one of the two α-like particles (21-22, 33-34) and (23-24, 35-36), which lie on the z axis and correspond to the $1d3/2$ states. It is the absence of the $1p1/2$ states (presented by the nucleon average positions numbered 9-10 and 15-16) from their structures (since ^{12}C is their core) which makes these six configurations have a very high excitation.

TABLE I. Vertex configuration, potential E_p, Coulomb E_C, kinetic $E_{\rm kin}$, spin-orbit $E_{\rm SO}$ binding energy E_B, excitation E_x energy, angular momentum and parity I_n^π values for nine configurations of ^{20}Ne. Each block of the table corresponds to a block of Fig. 2 and of Fig. 3 having the same letter labeling. Equivalent vertex configurations also are given next to the first one used for the construction of Figs. 2 and 3.

Core: ^{16}O (a)			Core: ^{16}O (b)		Core: ^{16}O (c)	
Valence: (17-18, 29-30) or (19-20,31-32)			Valence: (25-26, 37-38) or (27-28,39-40)		Valence:(21-22,33-34) or (23-24,35-36)	
$E_P=-\Sigma V_{ij}$	=	331.2	331.7		330.0	
$E_C=\Sigma^2 r_{ij}$	=	−18.5	−18.5		−18.5	
$E_{\rm kin}=\Sigma\langle T\rangle_{nlm}$	=	−153.4	−153.4		−153.4	
$E_{\rm SO}=\Sigma E_{(\rm so)_i}$	=	8.1	8.1		8.1	
E_B	=	167.4	167.9		166.2	
E_x(mod)	=	9.1	8.6		10.3	
E_x(exp)[a]	=	∼8.8	∼8.7		10.8±	
$\Gamma_{\rm c.m.}$>[a]	=	0.8	0.8		0.35	
I_n^+	=	2_4^+	O_4^+		4_4^+	

Core: ^{12}C (d)			Core: ^{12}C (e)		Core: ^{12}C (f)	
Valence: (17-18, 29-30) or (19-20,31-32)			Valence: (25-26,37-38), (27-28,39-40)		Valence: (21-22,33-34), (23-24,35-36)	
E_P	=	312.2	321.4	315.4	328.4	252.5	256.6
E_C	=	−17.0	−17.0	−17.0	−17.0	−17.0	−16.8
$E_{\rm kin}$	=	−159.3	−159.3	−159.3	−159.3	−159.3	−159.3
$E_{\rm SO}$	=	24.4	24.4	24.4	24.4	24.4	2.44
E_B	=	160.3	169.5	163.5	176.5	100.6	104.9
E_x(mod)	=	16.2	7.0	13.0	0.0	75.9	71.6
E_x(exp)[a]	=	16.4	6.7	13.2	0.0		
I_n^+	=	O_9^+	O_2^+	O_8^+	O_1^+		

Core: ^{12}C (g)				Core: ^{12}C (h)		Core: ^{12}C (i)	
Valence: (17-18,29-30),(25-26,37-38) or (17-18,29-30),(27-28,39-40) or (19-20,31-32),(25-26,37-38) or (19-20,31-32),(27-28,39-40)				Valence: (25-26,37-38),(21-22,33-34) or (25-26,37-38),(23-24,35-36) or (27-38,39-40),(21-22,33-34) or (27-28,39-40),(23-24,35-36)		Valence: (21-22,33-34),(17-18,29-30) or (21-22,33-34),(19-20,31-32) or (23-24,35-36),(17-18,39-40) or (23-24,35-36),(19-20,31-32)	
E_P	=	317.6	328.7	287.9	296.4	286.2	292.8
E_C	=	17.4	−17.3	−17.4	−17.2	−17.4	−17.2
$E_{\rm kin}$	=	−159.2	−159.3	−159.3	−159.3	−159.2	−159.2
$E_{\rm SO}$	=	24.4	24.4	24.4	24.4	24.4	24.4
E_B	=	165.4	176.5	135.6	144.3	134.0	140.8
E_x(mod)	=	11.1	0.0	40.9	32.2	42.5	34.7
E_x(exp)[a]	=	11.0	0.0				
I_n^+	=	O_5^+	O_1^+				

[a]See Ref. [2].

These configurations will not be discussed further in the paper. In contrast, for the configurations of Table I with excitation energies below 28.2 MeV, specific comments can be made based on Ref. [2]. Specifically, the excitation energy of configuration (b) 8.6 MeV is almost identical to the energy 8.7 MeV of the O_4^+ state, while that of configuration (d) relaxed 7.0 MeV is almost identical to 6.7 MeV of the O_2^+ state, and that of (g) 11.1 MeV is almost identical to 11.0 MeV of the O_5^+ state. In addition, the excitation energy of configuration (d) 16.2 MeV is almost identical to the experimental energy 16.25 MeV for which no spin and parity assignment has been made. That is, a new O^+ assignment could be made for this energy as a prediction of the present work. Finally, specific comments concerning the I^π assignment of configurations (a) and (c) with excitation 9.1 MeV and 10.3 MeV, respectively [2], will follow shortly. At this point, however, it is important to remark that all low-energy configurations (<28.2 MeV) of Table I (which exhaust all α-cluster structures predicted by the isomorphic shall model) are meaningful. That is, each of these configurations leads either to the g.s. or to an excited state with spin, parity, and energy experimentally supported. Above assignment, of course, refer to the excitation energy alone. However, they will be further supported below by employing additional observables.

As seen from Figs. 2 and 3, the existence of some deformation of the average shapes for ^{20}Ne in all parts of these figures is apparent. However, there is a substantial difference in deformation from configuration to configuration. Specifically, configurations (a)–(c) could be though of as possess-

ing a small prolate deformation (or even zero deformation if the valence α-like particle is considered rotating around the spherical ^{16}O core), while configurations (d)–(g) or (d) relaxed (g) relaxed could be thought of as possessing ''plane'' structure with significantly prolate deformation [see signs and values of Q'_{20} in Table V for the configurations (e) and (g)].

In the different parts of Fig. 2, the axes of symmetry and the corresponding axes of rotation also are shown. As explained in Refs. [30] and [31], here an axis of symmetry can be an axis of rotation as well, since none of these axes of symmetry has the C_∞ symmetry appearing, e.g., in an axially symmetric ellipsoidal. Thus, rotation around each of these symmetry axes is quantum mechanically permissible and could lead to an observable.

Table II lists five rotational bands, namely, the O_1^+, O_2^+, O_5^+, O_8^+, and O_9^+ bands, whose levels follow Eq. (16). Specifically, column 1 refers to the specific band name, while column 2 lists the relevant part of Fig. 2 and each of the remaining columns lists the I^π value (for $I=0,2,4,6,8$) and the corresponding energy and moment of inertia coming both from the experimental data and the present model.

Tables III and IV are similar to Tables I and II with the difference that they refer to three new bands (namely, O_3^+, O_6^+, and O_7^+) and to Fig. 4.

By applying Eqs. (5) and (6) and (8)–(11) the quantities $\langle r^2\rangle_{\rm ch}^{1/2}$, Q'_{20}, Q'_{30}, Q'_{40}, $B(E2)$, τ, β_2, and $\alpha_{\rm av}$ are computed and listed in Table V, columns 3–10 for the g.s. configurations (e) relaxed and (g) relaxed, together with the experimental data where available.

IV. DISCUSSION

Empirical assignment of rotational bands to ^{20}Ne exists in the literature [2] together with supporting [3.4] and objecting [5] criticism. The predictions of the present work are discussed below in relation to this literature by following a band-to-band development as in Ref. 1.

A. The O_1^+ band

In Ref. [2], which constitutes the latest compilation of the relevant data, the levels O^+, 2^+, 4^+, 6^+, 8^+ at the energies (in MeV) 0, 1.633674, 4.2477, 8.7776, and 11.951, respectively, have been assigned as unambiguous members of the ground state (g.s.) band.

As aforementioned, it is interesting that two different vertex (state) configurations are assigned [see Table I(e) and (g)] to the g.s. of ^{20}Ne and that both (e) and (g) configurations, as will be seen, are necessary for the description of the relevant observables. These configurations are depicted by Figs. 2(e) and (g), where their axes of symmetry (S) and rotation (R) considered in the calculations also are shown. The corresponding moment of inertia is listed in Table II underneath the predicted energy for each member state, together with the moment of inertia derived from the relevant experimental energy by using the formula $J_I=[\hbar^2 I(I+1)]/[2(E_I-E_0)]$. In these moment values the contribution of the nucleon finite size has been taken empirically equal to $0.165M$ fm^2,where M is the nucleon mass, as in Refs. [30] and [31].

By considering that each of these two configurations contribute equally (i.e., 50% each) to the excitation of the 2^+ state, the predicted excitation is 1.625 MeV, a value which compares very well with the experimental one 1.634 MeV. However, while for the first excited state the configurations of Fig. 2(e) and of Fig. 2(g) contribute equally to the energy, for the remaining states of the band the configuration of Fig. 2 (e) seems to be the main contributor, as noted numerically in Table II. Specifically, for the next two levels, i.e., 4^+ and 6^+, and by employing the same moments of inertia as for 2^+, i.e., 100.4 fm^2 and 61.9 fm^2 for the configurations of Fig. 2(e) and Fig. 2(g), respectively, one obtains the excitations 4.26 MeV and 8.78 MeV, respectively, which also compare very well with the experimental values 4.25 MeV and 8.78 MeV, respectively. For the 8^+ level the predicted energy is 11.99 MeV and the experimental one 11.95 MeV again in very good agreement. For this level the configuration of Fig. 2(e) participates 95%, while that of Fig. 2(g) 5%, and for the first configuration the moment of inertia is $J=131.5$ fm^2, while for the second it remains $J=61.9$ fm^2.

The change of the moment of inertia for the configuration of Fig. 2(e) means that the nucleons participating in the collective rotation include the eight $1p3/2$ nucleons of the ^{12}C core in addition to the eight $1d5/2$ valence nucleons participating in the excitation of the 2^+, 4^+, and 6^+ levels. That is, at 8^+ an additional shell (that of $1p3/2$ states) has been deformed and, thus, participates in the collective rotation. Hence, only the $1s$ shells remain spherical, behaving like a spectator with respect to the rotating part of the nucleus. This fact means that J_{8^+} has almost reached the solid-state limit, a fact which makes the prediction of the 10^+ member of this band rather easy by employing the same moments of inertia and a reasonable mixing of the configurations depicted by Fig. 2(e) and Fig. 2(g). Thus, for members of the band with $J^\pi>8^+$, it seems that an almost superdeformed band starts for ^{20}Ne. A test to this argument is to examine if another 8^+ level exists as a continuation of the lower deformation band. Indeed, such a model prediction at $E_{8^+}=15.88$ MeV could be taken as corresponding to the $E_{8^+}=15.874$ MeV experimental one suggested here for the first time. Now, the mixing is 89% for the configuration of Fig. 2(e) and 11% for that of Fig. 2(g).

B. The O_2^+ band

In Ref. 2, the levels 0^+, 2^+, 4^+, and 6^+ at the excitation energies (in MeV) 6.725, 7.4219, 9.990, and 12.585 or 13.105, respectively, have been assigned as members of the O_2^+ band. While the first three of these assignments (i.e., the 0^+, 2^+, and 4^+) are unambiguous, the last of the them (i.e., the 6^+) is in dispute, i.e., it is not clear which of the two 6^+ levels given above is more probable to be the correct member of this band. Also, while in the aforementioned compilation several 8^+ states are listed, none of them is assigned to the O_2^+ band, despite the fact that a definite proposition was made by Ref. [1] for the level 17.295 MeV based on arguments of reduced width, $\theta^2_{\alpha_0}$, for α emission to the ground state of ^{16}O (a fact suggesting the use of a cluster model approach for ^{20}Ne). The present approach, which is quite general and still a cluster approach, will probably shed some light on this intriguing matter.

TABLE II. Band head, relevant part of Fig. 2, I^{π}, excitation energy, and moment of inertia from experiments and model predictions for $I=0$, 2, 4, 6, and 8 of the rotational bands O_1^+, O_2^+, O_5^+, O_8^+, and O_9^+.

O_n^+ band	Vertex Config. Relevant part of Fig. 2	E_x (MeV±keV) exp[a]/mod 0^+ $J(\mathrm{fm}^2)$ exp[b]/mod	Γ (keV) τ_m	E_x (MeV±keV) exp[a]/mod 2^+ $J(\mathrm{fm}^2)$ exp[b]/mod	Γ (keV) τ_m	E_x (MeV±keV) exp[a]/mod 4^+ $J(\mathrm{fm}^2)$ exp[b]/mod	Γ (keV) τ_m	E_x (MeV±keV) exp[a]/mod 6^+ $J(\mathrm{fm}^2)$ exp[b]/mod	Γ (keV) τ_m	E_x (MeV±keV) exp[a]/mod 8^+ $J(\mathrm{fm}^2)$ exp[b]/mod	Γ (keV) τ_m
O_1^+		0.0000		1.63367±0.015	1.05 ps	4.2477±1.1	93 fs	8.7776±2.2	0.11	15.874±9	
	Fig. 2(e)			1.24*0.5=0.62		4.13*0.95=3.92		8.67*0.98=8.50		14.87*0.89=13.23	
	Fig. 2(g) relaxed			2.01*0.5=1.005		6.70*0.05=0.34		14.07*0.02=0.28		24.12*0.11=2.65	
				1.625		4.26		8.78		15.88	
						97.58		99.19		94.05	
	Fig. 2(e)			$J_x=100.4$		100.4		100.4		100.4	
	Fig. 2(g) relaxed			$J_x=61.9$							
										11.951±4	
										11.35*0.95=10.78	
										24.12*0.05=1.21	
										11.99	
										124.93	
										$J_x=131.5$	
										$J_x=61.9$	
O_2^+		6.725±5	19.0	7.4219±1.2	15.1						
	Fig. 2(d) relaxed	6.725		7.39		8.92					
				180.30							
				$J_x+J_y=189.54$		189.54					
						9.990±8	155	13.928±5	65	18.960±2.5	200
						10.06		13.72		18.72	
						127.21		120.90		122.02	
						$J_y=124.48$		124.48		124.48	
								13.105±5	102	17.295±15	200
								13.05		17.56	
								136.50		141.24	
								$J_y=137.74$		137.74	
								12.585±5	72	16.746±25	160
								12.48		16.59	
								148.61		148.98	
								$J_z=151.30$		151.30	
O_5^+		10.97±120	580	12.327±10	390	15.330±5	34	20.168±35	285	28	1600
	Fig. 2(g) normal	10.97		12.31		15.43		20.33		27.02	
				91.68		95.11		94.68		87.66	
				$J_x=93.04$		93.04		93.04		93.04	

TABLE II. *(Continued.)*

O_n^+ band	Vertex Config. Relevant part of Fig. 2	E_x (MeV±keV) exp[a]/mod 0^+ $J(\mathrm{fm}^2)$ exp[b]/mod	Γ (keV) τ_m	E_x (MeV±keV) exp[a]/mod 2^+ $J(\mathrm{fm}^2)$ exp[b]/mod	Γ (keV) τ_m	E_x (MeV±keV) exp[a]/mod 4^+ $J(\mathrm{fm}^2)$ exp[b]/mod	Γ (keV) τ_m	E_x(MeV±keV) exp[a]/mod 6^+ $J(\mathrm{fm}^2)$ exp[b]/mod	Γ (keV) τ_m	E_x (MeV±keV) exp[a]/mod 8^+ $J(\mathrm{fm}^2)$ exp[b]/mod	Γ (keV) τ_m
				12.221±4	<1	''15.330±5''	34	20.027±15	80		
				12.26		15.28		20.03		26.50	
				99.45		95.11		96.15			
				J_y=96.14		96.14		96.14		96.14	
						13.048±5	18	15.70±15		18.960±25**	200
						13.19		15.64		18.97	
						J_x+J_y=199.57		184.12		186.85	
						186.54		186.54		186.54	
O_8^+		13.222±10	40	14.115±5	42	16.329±11	45	19.845±40	360	24.9±500	broad
	Fig. 2(e) normal	13.0		14.17		16.37		19.84		24.57	
				139.32		133.47		131.49		127.84	
				J_x=131.54		131.54		131.54		131.54	
				13.908±5	74	15.330±5*	34	18.286±10	190		
				13.90		15.48		17.97		21.36	
				181.36		196.73		171.97			
				J_x+J_y=183.34		183.34		183.34		183.34	
O_9^+		''15.82''		16.437±11	35	18.083±25	140	20.419±30	25	23.4±200	500
	Fig. 2(d) normal	15.82		16.48		18.01		20.41		23.70	
				201.64		183.25		189.36		196.96	
				J_x+J_y=189.54		189.54		189.54		189.54	

[a]See Ref. [2].
[b]See Ref. [2] and Eq. (6).

TABLE III. Same structure and notations as in Table I, but for the three configurations of Fig. 4.

Core: ^{12}C			Core: ^{16}O	Core: ^{16}O
Valence: (17-18,29-30),(25-26),(31-32) or (17-18,29-30),(27-28),(31-32) or (19-20,31-32),(25-26),(29-30) or (19-20,31-32),(27-28),(29-30)			Valence: (25,38),(27,40) or (25,37),(27,30) or (26,38),(28,40) or (26,37),(28,39)	Valence: (17,29),(19,31) or (17,30),(19,32) or (18,29),(20,31) or (18,30),(20,32)
$E_P=-\Sigma V_{ij}$	=	321.1	328.7	327.2
$E_C=-\Sigma e^2/r_{ij}$	=	−17.0	−18.3	−18.3
$E_{\rm kin}=\Sigma\langle T\rangle_{nlm}$	=	−159.3	−153.4	−153.4
$E_{\rm SO}=\Sigma E_{(\rm SO)_i}$	=	24.4	8.1	8.1
E_B	=	169.2	165.1	163.8
E_x(mod)	=	7.3	11.4	12.8
E_x(exp)[a]	=	7.2	11.6	12.4
I_n^+	=	O_3^+	O_6^+	O_7^+

[a]See Ref. [2].

In Fig. 2(d) relaxed, standing for the average structure of the O_2^+ level, the symmetry axis (S) and the rotation axes (R) are shown, and, thus, the corresponding moments of inertia can be computed easily if the rotating nucleons are specified. The predicted excitation energies, in very good agreement with the experimental data, and the corresponding moments of inertia are given in Table II. As stated there, different axes of rotation and a different number of rotating nucleons have been considered for the derivation of the predicted energies and their corresponding moments of inertia.

Specifically, for the 2^+ level the rotating nucleons are the eight $1d5/2$ valence nucleons plus the eight $1p3/2$ nucleons of the ^{12}C core. A simultaneous rotation of these 16 nucleons around both the x and the y axes takes place. For the 4^+ and 6^+ levels the rotation takes place around the y axis alone. However, the rotating nucleons for the 4^+ level include the valence nucleons plus the $1p3/2$ protons, while for the 6^+ level at 13.105 MeV, in addition, the $1p3/2$ neutrons rotate.

The second 6^+ level at 12.585 MeV also is supported by the present study which predicts a state at 12.48 MeV by considering that all nucleons rotate around the z axis. An even third 6^+ level is predicted here at 13.72 MeV in good agreement with the experimental 6^+ level at 13.928 MeV. This new level belongs to the same branch as the aforementioned 4^+ level at 9.990 MeV possessing the same moment of inertia 124.48 fm^2 (see Table II). It is interesting that this third 6^+ level also has been proposed by Ref. [45] despite the fact that it is not included in the compilation of Ref. [2] as a member of the O_2^+ band. The $\theta^2_{\alpha_0}$ value agrees with this third 6^+ level as well [1]. The support here of all these three 6^+ levels as member states of different branches of the O_2^+ band compromises all conflict in the literature [1,4,45–49]. Thus finally, the O_2^+ band appears to have a total of four branches—the first with moment of inertia $J=189.54$ fm^2, the second with $J=124.48$ fm^2, the third with $J=137.74$ fm^2, and the fourth with $J=151.30$ fm^2 (see Table II). Rotation around the symmetry axis x, used above for the calculation of the moment of inertia for the first branch, is meaningful here as has been explained earlier [30,31]. Apparently, the fourth branch is a superdeformed band since all twenty nucleons rotate.

Predicting the 8^+ member states of the superdeformed and the two lower deformation bands, one obtains the energies (in MeV) 16.59, 17.56, and 18.72 (by using for each 8^+ level the same moment of inertia as the corresponding 6^+ member state [see Table II], which compare very well with the experimental ones (in MeV) 16.746, 17.295, and 18.690, respectively. These predicted levels possess the correct spin and parity. The prediction here that the level 17.294 MeV is a member of the O_2^+ band is consistent with Refs. [1,50,51] and, thus, is in contrast with Ref. [49] which argues that this level belongs to the O_4^+ band. The present study is also in agreement with Ref. [1] concerning the 8^+ level, 15.9 MeV, thus, this level does not belong to the O_2^+ band as suggested by Ref. [45].

The use of ^{12}C as a core for the explanation of this and the previous O_1^+ bands is supported by Ref. [52], where explanations of these bands were given by considering ^{12}C+^{8}Be as α-cluster-type structure.

The explanation [31] of using sometimes different axes of rotation for different levels in light nuclei is that a light nucleus meets some difficulty in starting a rotational band, a situation which shows up in a rotation of the nucleus around an axis which is not the one with the maximum moment of inertia. As the excitation of the nucleus gets larger, however, the rotation may change axis corresponding to a larger moment of inertia. Such behavior is very well known in classical physics in describing the different stages of rotation of a triaxial solid body.

A second situation described above, where a moment of inertia increases suddenly at a certain excitation energy of a nucleus, is the one where deformation of one or more additional shells (from the outermost to the innermost) occurs suddenly at that energy, a fact which leads to the participation of this or these shells in the collective rotation leading to a sudden increase of the moment of inertia.

C. The O_4^+ band

The main characteristic of the band is that the reduced widths of the 0^+2^+, and 4^+ states (which are the only member states established) for an α emission to the ground state of ^{16}O, namely $\theta^2_{\alpha_0}=0.70,\ 0.95$, and 0.33, respectively, are nearly the single particle limits [1], and, thus, they do not favor a rotational band.

TABLE IV. Same structure and notations as in Table II, but for the rotational bands O_3^+, O_6^+, and O_7^+ corresponding to the relevant parts of Fig. 4.

O_n^+ band	Vertex Config.	E_x (MeV±keV) exp[a]/mod 0^+ J(fm^2) exp[b]/mod	Γ (keV) τ_m	E_x (MeV±keV) exp[a]/mod 2^+ J(fm^2) exp[b]	Γ (keV) τ_m	E_x (MeV±keV) exp[a]/mod 4^+ J(fm^2) exp[b]/mod	Γ (keV) τ_m	E_x (MeV±keV) exp[a]/mod 6^+ J(fm^2) exp[b]/mod	Γ (keV) τ_m	E_x (MeV±keV) exp[a]/mod 8^+ J(fm^2) exp[b]/mod	Γ (keV) τ_m
O_3^+		7.191±3	3.4	7.829±2.4	2			12.137±5		15.78	
	Fig. 3(a) rel.	7.19		7.86		9.41		11.85			
				195.0							
				J_x+J_y=186.9		186.9					
						9.031±7	3				
						9.03		11.06		13.83	
						225.38					
						J_x+J_z=225.0		225.0			
O_6^+		11.558±4	1.1	''12.221±4''	<1	13.965±5	8.1	16.505±15	24		
	Fig. 3(b)	11.56		12.27		13.94		16.55		20.12	
				187.65		172.29		176.04			
				J_x+J_y=174.3		174.3		174.3		174.3	
										18.621±20	185
										18.44	
										211.37	
										J_x+J_z=216.8	
O_7^+		12.433±5	24.4	12.957±5	38	''14.270''±10	92	''16.871''±20	350	''19.731''±20	330
	Fig. 3(c)	12.43		13.01		14.35		16.45		19.32	
				234.74		225.75		196.23		204.57	
				J_x+J_z=216.8		216.8		216.8		216.8	

[a]See Ref. [2].
[b]See Ref. [2] and Eq. (6).

TABLE V. Model employed, binding energy, charge root mean square radius $\langle r^2\rangle_{\rm ch}^{1/2}$, electric quadrupole Q'_{20}, octupole Q'_{30}, and hexadecapole Q'_{40} moment, reduced electric quadrupole transition $B_{E(2)}$ mean lifetime τ, deformation parameter β_2, and average moment of inertia factor $\alpha_{\rm av}$ for the g.s. of ^{20}Ne together with experimental values.

	E_B (MeV)	$(\langle r^2\rangle_{\rm ch}^{1/2})$ fm	Q'_{20} $e\cdot fm^2$	Q'_{30} $e\cdot$fm^3	Q'_{40} $e\cdot$fm^4	B_{E2} $e\cdot$fm^4	τ ps	β_2	$\alpha_{\rm AV}$
Isomorphic Shell Model									
a) Fig. 2(e), sym. axis y	176.5	3.13	102.8		2810				
b) Fig. 2 (g), sym. axis y	176.5	3.13	33.1		2351				
50% occupancy of a,b	176.5	3.13	68.0		2581	459	0.76	0.85	0.218
exp	160.65[a]		80.5±10.5[b]			480±90[c]	0.73[c]	0.87[c]	
HF with LINEG interaction [d]	143.0	3.05	49.8			247[e]	1.42[e]	0.62[e]	
HF with B1 interaction[d]	112.4	3.04	47.8			227[e]	1.54[e]	0.60[e]	
HF with band-mixed[b]			56.0			312[e]	1.12[e]	0.70[e]	
HF various calculations[b]			30.5-63.0			93-395[e]	3.8-0.89[e]	0.38-0.78[e]	
SM various calculations[b]			44.8-57.1			200-324[e]	1.8-1.08[e]	0.56-0.71[e]	
Rotational model[b]			57.8±1.8			312-353[e]	1.12-0.99[e]	0.70-0.74[e]	
Skyrme-type formulas[f]									0.200[f]

[a]See Ref. [63].
[b]See Ref. [64].
[c]See Ref. [42].
[d]See Ref. [65].
[e]Derived from Q'_{20} by using Eq. (23).
[f]$\alpha_{\rm av}=\Sigma_I\alpha_I(2I+1)/\Sigma_I(2I+1)$; see Ref. [66].

In the framework of the isomorphic shell model, each of these three levels corresponds to a different average structure [see Figs. 2(a)–(c), and Table I(a)–(c), respectively] and, in this sense, possesses a shell model intrinsic state. This is well supported by the fact that the predicted binding energies (in MeV), i.e., 8.6 (8.7), 9.1 (8.8), and 10.3 (10.8), respectively, which are in good agreement with the experimental data (given above inside parentheses), as derived strictly by considering single particle components of the energy or, in other words, without considering any collective rotational component [see Eq. (16)]. Furthermore, while each of these three average structures has a ^{16}O core and four valence nucleons forming an α-like particle, these structures resemble a dinuclear molecular type of structure, but they cannot be seen as an α cluster orbiting around a ^{16}O core, first because the α, ^{16}O separation distance is rather short (equal to 3.361 fm and not 4.6– 4.9 fm, as suggested by Fujiwara [4]) and second because, as seen from Table I and already mentioned above, no rotational component is employed for a good reproduction of each corresponding excitation energy. Thus according to the present study, the existence of a O_4^+ rotational band does not have physical support. In fact, Tomoda and Arima [3] suggest that the state 4^+, 10.8 MeV, may not belong to the O_4^+ band. Also, in Ref. [1] some doubts have been expressed concerning the existence of members of this band with $I^\pi\geqslant 4^+$. In addition, the ^{16}O+α cluster-type structure for the states O^+, 2^+, and 4^+ of the O_4^+ ''band'' is supported by Ref. [53] in agreement with the present study.

D. The O_5^+ band

In Fig. 2(g) the average structure assigned to O_5^+ is shown, together with the symmetry axis (y) and the rotational axes (x) and (y). The proton average positions numbered 3 and 4 in Fig. 2(g) are at their ''normal'' (not ''relaxed'') places.

The model prediction for the 2^+ level is 12.31 (12.33) MeV and corresponds to a moment of inertia equal to 93.04 fm^2. This moment of inertia assumes a rotation of both the 8 valence nucleons in the $1d5/2$ subshells and of the 8 nucleons in the $1p3/2$ subshells [while the $1p1/2$ subshells are empty since ^{12}C is the core in Fig. 2(g)]. This energy prediction is in very good agreement with the experimental value 12.327 MeV, whose reduced width $\theta^2_{\alpha_0}=0.08\pm0.02$ is also in the expected relationship with that of the O_5^+ level, namely 0.14. Moment of inertia prediction is in good agreement with the experimental one 91.68 fm^2 (see Table II).

For the higher member states with $I^\pi=4^+$, 6^+, and 8^+ at energies (in MeV) 13.048, 15.70, 18.960, respectively (tentatively assigned by Ref. [1] to the O_5^+ band even though their assignment is not included in the latest compilation of Ref. [2], where the 6^+ state appears as doubtful), our predictions are (in MeV) 13.19, 15.64, and 18.97, respectively. Thus, the present predictions support the previous tentative assignment [1] and, in addition resolve some dilemma in the choice of nearby energies having the same spin and parity. These predictions result by using $J=186.54$ fm^2 as the moment of inertia for all of them, which is close to the experimental value 199.57 fm^2. In evaluating this moment of inertia, it is assumed that a rotation takes place simultaneously around the axes x and y of both the 8 $1d5/2$ valence nucleons and the 8 $1p3/2$ nucleons of the ^{12}C core. It should be mentioned that the 8^+, 18.960 MeV level also has been discussed here earlier as a possible member state of the O_2^+ band, a conflict which should be clarified in later studies. Perhaps, there is another 8^+ state at an energy close by.

The above three levels belong to an almost superdeformed branch of the band since only the 4 nucleons of the $1s$ states remain as spectators to the collective rotation of all other nucleons. Thus the 2^+ level at 12.327 MeV (which is the

only level assigned by the compilation of Ref. [2] to the O_5^+ band) belongs to a branch of the band of lower deformation.

It is interesting to examine if there are other states of this branch. Indeed, by employing $J_{2^+}=93.04$ fm^2 as the moment of inertia of all members of this branch higher than 2^+, we obtain for the energies (in MeV) of $I^\pi=4^+$, 6^+, and 8^+ 15.43 (15.330), 20.33 (20.168), and 27.02 (28), respectively, where inside parentheses the experimental energies (with the correct spin and parity) are given. The agreements between predictions and data are very good except for the 8^+ level where, of course, $\Gamma_{\text{c.m.}}=1.6$ MeV, a fact which smoothes the impression resulting from the rather larger deviation of 0.98 MeV between theory and experiments. Thus these three levels are reasonable predictions of the present model and are not included in Ref. [1].

Finally, an additional branch of the O_5^+ band is suggested here based on a moment of inertia $J=96.14$ fm^2 which involves the same nucleons, as the previously discussed lower deformation branch, but the rotation now takes place around the axis y (see Table II). The predicted energies are (in MeV) 12.26, 15.28, 20.03, and 26.50 for $I^\pi=2^+$, 4^+, 6^+, and 8^+, respectively. These predictions for the first three levels are supported (in location and spin-parity assignment) by the experimental energies (in MeV) 12.221, 15.330, and 20.027. The prediction for the 8^+ is beyond the present knowledge of the ^{20}Ne energy spectrum. It should be noted, however, that the level 4^+, 15.330 MeV also has been assigned in the previous lower deformation band. Perhaps, another 4^+ level exists in a nearby energy.

Thus in the present study, three different branches are suggested for the O_5^+ band of a total of 10 member states supported experimentally, while in the compilation of Ref. [2] only one level was assigned to this band.

E. The O_8^+ and O_9^+ bands

These two bands are introduced here for the first time. The average structures assigned by the model to their intrinsic states are shown in Figs 2(e) and (d), respectively. Their corresponding band head energies are given in Table I blocks (e) and (d), respectively, together with their core and valence vertex (state) configurations. For both bands the proton average positions numbered 3 and 4 are at their ''normal'' (not ''relaxed'') places.

While in the literature not even one level has been assigned to these two bands, the model employed here is able to predict moments of inertia by using the symmetry properties of the relevant vertex configuration for each band. Without any reference to the experimental energies (used only for comparison), the model makes successfully real predictions by employing these moments of inertia.

Specifically, the axes of rotation, their moments of inertia, and their corresponding rotational spectra for both the O_8^+ and the O_9^+ bands are given in Table II together with supporting experimental data possessing the correct spin and parity. In both rotational spectra, the maximum deviations appear at the $I^\pi=8^+$ levels. However, at these two levels there are large experimental errors and large values of $\Gamma_{\text{c.m.}}$ enough to compensate for the difference, which does not exceed 0.33 MeV. Indeed, the agreements between model predictions and supporting experimental data are very good.

Totally, the O_8^+ band has two branches, while the O_9^+ band has only one. The moments of inertia listed in Table II for these two bands came by rotation around the axes listed in this table and correspond to the following rotating parts of ^{20}Ne. O_8^+ band: $J=131.54$ fm^2 corresponds to the rotation of the valence nucleons and of the $1p3/2$ core nucleons around the x axis, while $J=183.34$ fm^2 corresponds to the rotation of the same nucleons, but simultaneously around both x and y axis. O_9 band: $J=189.54$ fm^2 corresponds to the rotation of the valence nucleons and of the $1p3/2$ core nucleons simultaneously around both the x and y axes.

F. The O_3^+, O_6^+, and O_7^+ bands

These three bands are slightly out of the scope of the present paper which deals mainly with average structures of ^{20}Ne made of only α-like particles. Indeed, the O_3^+, O_6^+, and O_7^+ bands whose average structures of their intrinsic states are shown in Figs. 3(a)–(c), respectively, besides may be one (at maximum) valence α-like particle possess at least one valence pair of protons and one valence pair of neutrons which do not form an α-like particle since their average positions are far apart. Specifically, only the O_3^+ band possesses one valence α-like particle, while the O_6^+ and O_7^+ bands possess only pairs of valence nucleons. This situation is consistent with the comment of Ref. [1] that the O_3^+ band has a smaller reduced width, $\theta^2_{\alpha_0}$, for an α emission to the ground state of ^{16}O than the O_2^+ band, which here is composed from α-like particles alone.

For reasons of completeness, however, these three bands also are included in the present study. Specifically, in Figs. 3(a)–(c) and Tables III and IV (whose explanations are similar to Fig. 2 and Tables I and II, respectively) the average intrinsic structures together with the relevant symmetry and rotational axes, and the model predictions for the energies and the corresponding rotational bands with their moments of inertia are given for each of these three bands. The agreements between model predictions and experimental data of Ref. [2] are very good, except for the 6^+ of the O_7^+ band at 19.443 MeV, which is a doubtful assignment and is not supported by the present study. However, some interesting points require further discussion.

For all these three bands the moments of inertia used come as the sum of two moments of inertia around two perpendicular axes (see Table IV).

It is worth noticing that in all these three bands *all* nucleons of ^{20}Ne participate in the collective rotation, a situation characteristic of superdeformation as has been already commented on earlier for similar cases. This makes the predictions for higher excitations on each branch rather secure, since no further increase of the moment of inertia is possible. The increase of the moment of inertia between branches listed in Table IV for the O_3^+ and O_6^+ bands comes by changing the combination among the x,y,z axes of the specific two axes employed in the rotation and not by changing the number of nucleons participating in the collective rotation.

The use of ^{12}C as a core for the explanation of the O_3^+ band is consistent with Ref. [54], where for this explanation a ^{12}C+^{8}Be α cluster-type structure is employed. Also, it is

consistent with the more general Ref. [54], where four p particles are raised up to the next shell (s,d orbits) to explain the O_2^+ state in ^{16}O, in analogy to the low lying $\frac{1}{2}^-$ state in ^{19}F and the $\frac{1}{2}^-$ state at around 3 MeV excitation of ^{17}O and ^{17}F [14].

For the 4^+ state of the lower deformation branch of the O_3^+ band predicted at 9.41 MeV, no experimental counterpart exists. The 2^+ state of the O_6^+ band and the states 4^+, 6^+, 8^+ of the O_7^+ band are for the first time here assigned to experimental energies (in MeV), i.e., 12.221, 14.270, 16.871, and 19.731.

The structure of the average intrinsic state of the O_7^+, made here of a ^{16}O core plus two pairs of nucleons which do not form an α-like particle, is supported by the fact that $\theta^2_{\alpha_0} \approx 0.001$, i.e., there is a large structural impossibility of decay of the O_3^+ state of ^{20}Ne into $\alpha + {}^{16}O_{g.s.}$ [55].

G. Spurious states

As known, in the shell-model approach, like the one described in [7a], the interparticle potential W in Eq. (25)

$$H=\sum_{i=1}^{A} T(i)+\sum_{l=i<j}^{A} W(r(i)-r(j)) \tag{25}$$

is replaced by a sum of central single-particle potentials, $\sum_i u(r(i))$, that are fixed in space, and a residual interaction. Hence the resulting shell-model Hamiltonian is no longer invariant with respect to translations and, thus, the calculated wave functions may contain unphysical, spurious components which describe excitations of the center-of-mass motion of the nucleus possessing no physical interest.

It is noticeable that the harmonic-oscillator potential used in Eq. (3) is the only potential which permits the partition into a center-of-mass Hamiltonian and a Hamiltonian for the relative motion. For such a potential all wave functions with the lowest energy allowed by the Pauli exclusion principle are completely nonspurious. However excitations of one or more particles into higher orbits may introduce spuriosity. Several methods have been derived to treat the problem of the removal of spurious states.

The present work, however, employs the semiclassical part of the isomorphic shell model [6], where a two-body potential (12) is applied among all nucleons pairs for the ground state and the excited states of ^{20}Ne. That is, the many body problem of this nucleus is described in terms of relative coordinates and, thus, only intrinsic excitations are involved corresponding to the genuine excitations of the physical system related to those observed experimentally. Hence spurious, unphysical components, due to excitations of the center-of-mass motion, do not sneak in the present results neither in the ground state nor in the excited states.

IV. COMPARISON WITH RESULTS OF OTHER MODELS

In Table V one can see the predictions of the present model for the observables of binding energy E_B, rms charge radius $\langle r^2\rangle^{1/2}_{ch}$, electric quadrupole moment Q'_{20}, electric octupole moment Q'_{30}, electric hexadecapole moment Q'_{40}, reduced electric quadrupole transition rate for the g.s. to 2^+ state transition $[B(E2)]$, mean lifetime τ, deformation parameter β_2, and the average moment of inertia α_{av} for the g.s. of ^{20}Ne, together with experimental data and predictions of other models for comparison. The different models employed here are listed in column 1 of the table, while the relevant references are cited as footnotes of this table. The abbreviations HF, LINEG, B1, and SM used in the table stand for Hartree-Fock, Negele, Brink, and Shell Model.

First one should notice that the predictions of the present approach on all observables are the average values of these observables coming from the vertex (state) configurations depicted by Fig. 2(e) relaxed and Fig. 2(g) relaxed. These configurations have identical binding energies and, as aforementioned, are considered to contribute 50% each to all g.s. observables of ^{20}Ne.

It is apparent from Table V that the predictions of the present approach approximate the experimental data closer than any other approach employed here. The largest deviation appears for the binding energy, where the approach using LINEG interaction gives almost equal deviation. However this latter approach gives larger deviations for all other observables of Table V. The ability of the present approach to predict simultaneously good results for many observables, without using adjustable parameters, constitutes a unique character of the isomorphic shell model employed here. Moreover, the present approach has the advantage of presenting the physical structure of the states. Indeed, in other models, with the exception of the calculations performed with an SU(3)-classified basis [56], the resulting eigenvectors consist, namely, of a very large number of small components. It is, therefore, highly impractical to extract information from these models on such structural properties as intrinsic deformation, orbital symmetry, α clustering, etc. which are quite important for the sd-shell nuclei [57].

Furthermore, it is interesting for one to notice that certain symmetries of Fig. 2 can follow from two simple and well-known properties of all effective shell-model interactions, namely, the exchange nature and the finite range [58]. In addition, the deformed intrinsic states presented by Fig. 2 could be used in any HF treatment of the relevant rotational bands, a fact which, obviously, relaxes the requirement of rotational invariance for the HF density [58].

An additional interesting feature of the average g.s. structures studied in Table V is the hexadecapole deformation of these structures for ^{20}Ne (see Q'_{40} values), a fact which is verified experimentally by the scattering of α particles on this nucleus [59]. If Fig. (g) relaxed, however, is considered alone, the existence of octupole deformation is apparent, something which is supported by Refs. [60–62]. The results there demonstrate clearly the necessity of including the left-right asymmetric degrees of freedom in self-consistent calculations aiming at an accurate description of the spectroscopy of ^{20}Ne. Indeed, there [60], the collective path is defined in terms of a combination of quadrupole and octupole moments, exactly as in the present study, where Fig. 2(e) relaxed stands for the quadrupole and Fig. 2(g) relaxed for the octupole moment.

V. CONCLUSIONS

The semiclassical part of the isomorphic shell model (whose main features are that it is a microscopic nuclear-

structure model which incorporates into a hybrid model the prominent features of shell model and liquid drop models in conjunction with the nucleon finite size and that the model uses no adjustable parameters) has been employed for the study of nine O_n^+ states and their rotational bands of ^{20}Ne. The results have been compared successfully with experimental data and those of other models.

Persisting ''α''-planar structure has been found for ^{20}Ne when the center of gravity of each α-like particle in the model is considered. Specifically, out of the nine O_n^+ states examined, six possess planar average structures. The remaining three O_n^+ states have three-dimensional average structures. Two out of these three and one out of the previous six have mixed structures made of α-like particles and one (minimum) or two (maximum) pairs of nucleons, while the remaining six have average structures strictly made of α-like particles. Of course, in later moments all nine of them evolve according to the independent particle motion of their constituent nucleons. Two-dimensional (planar) structure means here that the core is ^{12}C, while for a three-dimensional structure the core is ^{16}O.

It is noticeable that two different ''α''-planar structures have been associated with the g.s. of ^{20}Ne and that the different g.s. observables have been calculated as a mixture of these two configurations. However, while for the O_1^+ and 2_1^+ states this mixture is 50% of each, for the other members of the g.s. band the one configuration becomes dominant.

In calculating the moments of inertia, it has been found that the number of nucleons participating in collective rotation may vary and may become larger at higher member states of the same band. Each time the moment of inertia varies in a band, a new branch of the band starts. The moments of inertia of two different branches of a band differ by the moment of inertia of complete (deformed) shells from the outermost to the innermost. In other words, when part of the core participates in the collective rotation, the nucleons of *whole* shells are involved successively from the outermost to the innermost shell. This means that as the excitation of the nucleons gets larger and larger, at a certain energy *whole* shells (successively from the outermost to the innermost) get deformed and start participating in the collective rotation. Thus, the moment of inertia increases from branch to branch. An exception to this rule is the moment of inertia of the 2^+ state of the O_2^+ band which is larger than those of all other higher spin members of the band. This exception favors the existence of additional 2^+ states at energies larger than 7.4219 MeV as members of this band with moments of inertia smaller than 189.54 fm^2.

Another interesting feature of the moments of inertia in ^{20}Ne is that different axes of rotation have been employed for different members of the same band. This change follows the rule that each time the axis of rotation changes in going from one branch to another branch of the same band, the new axis should lead to a larger moment of inertia. This behavior is familiar from the classical rotation of a rigid body possessing three-axial symmetry. Both above features leading to a variation of the moment of inertia from branch to branch of the same band have been met for the first time in Ref. [31].

A third feature met here for the first time is that a collective rotation could take place simultaneously around two perpendicular axes and this is a third way of increasing the moment of inertia from branch to branch of the same band.

Situations of superdeformation have been noticed for the branches of the bands where the moment of inertia gets its largest possible value in the band. For these situations all nucleons, or almost all nucleons, of ^{20}Ne participate in the collective rotation.

Many new experimental states, even whole new branches of states, have been assigned as members of known rotational bands. Additionally, two completely new rotational bands (the O_8^+ and O_9^+) have been introduced here for first time, a fact which demonstrates the power of the employed model. Indeed, in the framework of the semiclassical part of the isomorphic shell model, a moment of inertia can be estimated without the knowledge of rotational levels being necessary. A moment of inertia can be estimated directly from the symmetry properties of the shapshot of the nucleon average positions constituting a specific band head. A snapshot is completely determined from its binding energy in relation to the snapshot of maximum binding energy taken as the ground state configuration.

The O_4^+ rotational band [1], according to the present study, has no physical support. Its states are interpreted as shell model states with a different average structure each. Criticism concerning its states with $I^\pi \geq 4$ exists in the literature [1,3], where one also may find support [53] for the ^{16}O$+\alpha$ cluster-type structure supported here.

Also of interest is the fact that rotational branches of the same or different bands of ^{20}Ne have almost the same moment of inertia, something which has been observed in the study of nuclei in the well-deformed region and, particularly, in the cases of nuclei with superdeformation.

Quadrupole, octupole, and hexadecapole deformations have been determined in ^{20}Ne in consistency with Refs. [60] and [59], respectively.

The present study supports strongly an α-like particle composition of the ground state and many excited states of ^{20}Ne. It is noticeable that any α cluster arrangement supported by the model leads to an observable. However, in moments later than that depicted in Figs. 2 and 4, where an α

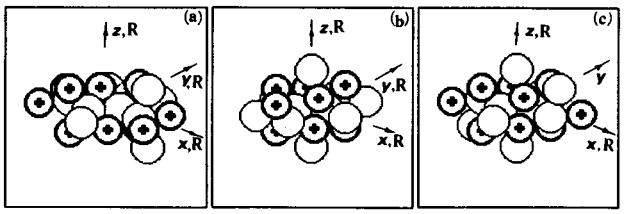

FIG. 4. Average forms of ^{20}Ne, according to the isomorphic shell model, composed of average positions of the constituent nucleons (NAP) forming an ''α'' particle or pairs of nucleons (two protons or two neutrons). (a) ^{12}C core (NAP 1-8, 11-16) plus one ''α'' particle (NAP 17-18, 29-30), one pair of neutrons (25-26), and one pair of protons (31-32). (b) ^{16}O core (NAP 1-16) plus two pairs of one neutron and of one proton (NAP 25, 38; 27,40), (c) ^{16}O core plus two different pairs of one neutron and of one proton (NAP 17,29; 19,31). Part (a) could be presented by a plane if ''α'' particle and pairs of nucleons are substituted by their center of gravity. This is not valid for parts (b) and (c). For part (a) the average positions of the 1s protons are considered at their ''relaxed'' location. Numbering of NAP and labeling of axes as in Figs. 1 and 2.

structure of ^{20}Ne is apparent, each constituent nucleon follows its independent particle motion in a well-defined shell model orbital.

The present approach has the unique advantages that first it can determine all observables starting from the configuration of the nucleon average positions which results directly from the assumptions of the employed model without using adjustable parameters, and second it provides information about the intrinsic structure of the states with no reference to the experimental data. Indeed, it is of interest and remains an open question whether we can obtain unambiguous information on the nuclear shape from the analysis of the experimental data. In experiments using strongly interacting probes, there are ambiguities of the optical potential which do not provide directly information on the nuclear shapes of target nuclei.

As apparent from Table V, the predictions of the present work are superior to those coming from other approaches. In general, the present work stands for the most exhaustive study of ^{20}Ne in the literature.

ACKNOWLEDGMENTS

One of us (G. S. A.) wants to express deep appreciation to Dr. P. E. Hodgson of the Nuclear Physics Laboratory (University of Oxford) for his valuable help in all stages of this research. Also it is his pleasure to thank Dr. A. C. Merchant of the Nuclear Physics Laboratory (University of Oxford) for valuable discussions. Finally, he wants to thank the Nuclear Physics Laboratory for its hospitality and also the NCSR ''Demokritos'' for financial support during his sabbatical leave. This work was supported in part by funds provided by the Empeirikeion Foundation, Panepistimiou 6, 106 71 Athens, Greece.

[1] H. T. Richards, Phys. Rev. C **29**, 276 (1984).
[2] F. Ajzenberg-Selove, Nucl. Phys. **A475**, 1 (1987).
[3] T. Tomoda and A. Arima, Nucl. Phys. **A303**, 217 (1978).
[4] Y. Fujiwara, H. Horiuchi, K. Ikeda, M. Kamimura, K. Sato, Y. Suzuki, and E. Uegaki, Prog. Theor. Phys. Suppl. **68**, 109 (1980).
[5] M. Bouten, M. C. Bouten, and E. Courier, Nucl. Phys. **A193**, 49 (1972).
[6] G. S. Anagnostatos, Int. J. Theor. Phys. **24**, 579 (1985).
[7] (a) G. S. Anagnostatos, Can. J. Phys. **70**, 361 (1992). (b) M. K. Gaidarov, A. N. Antonov, G. S. Anagnostatos, S. E. Massen, M. V. Stoitsov, and P. E. Hodgson, Phys. Rev. C **52**, 3026 (1995).
[8] J. A. Wheeler, Phys. Rev. **32**, 1083 (1937).
[9] W. Wefelmeier, Z. Phys. **107**, 332 (1937).
[10] D. Dennison, Phys. Rev. **57**, 454 (1940).
[11] J. M. Blatt and V. F. Weisskopf, *Theoretical Nuclear Physics* (Wiley, New York, 1952), p. 292.
[12] D. Dennison, Phys. Rev. **96**, 378 (1954).
[13] S. L. Kemeny, Phys. Rev. **103**, 358 (1956).
[14] H. Morinaga, Phys. Rev. **101**, 254 (1956); Phys. Lett. **21**, 78 (1966).
[15] K. Wildermuth and Th. Kanellopoulos, Nucl. Phys. **7**, 150 (1958); **9**, 449 (1958).
[16] D. M. Brink, in *The Alpha-Particle Model of Light Nuclei*, Proceedings of the International School of Physics, ''Enrico Fermi,'' Course XXXVI, edited by C. Bloch (Academic, New York, 1966).
[17] K. Ikeda, N. Takigawa, and H. Horiuchi, Suppl. Prog. Theor. Phys. **42**, 464 (1968).
[18] D. M. Brink, H. Friedrich, A. Weiguny, and C. W. Wong, Phys. Lett. **33B**, 143 (1970).
[19] D. Robson, Phys. Rev. Lett. **42**, 876 (1979).
[20] D. Robson, Phys. Rev. C **25**, 1046 (1984).
[21] W. Bauhoff, H. Schultheis, and R. Schultheis, Phys. Lett. **95B**, 5 (1980); **106B**, 278 (1981); Phys. Rev. C **22**, 861 (1980); **29**, 1046 (1984).
[22] S. Marsh and W. D. M. Rae, Phys. Lett. B **180**, 185 (1986).
[23] P. E. Hodgson, in *Atomic and Nuclear Clusters*, Proceedings of the Second International Conference at Santorini, Greece, 1993, edited by G. S. Anagnostatos and W. von Oertzen (Springer, Berlin, 1995); Cont. Phys. **35**, 329 (1994).
[24] A. C. Merchant and W. D. M. Rae, Nucl. Phys. **A549**, 431 (1992).
[25] W. D. M. Rae and A. C. Merchant, Mod. Phys. Lett. A **8**, 2435 (1993).
[26] J. Zhang and W. D. M. Rae, Nucl. Phys. **A564**, 252 (1993).
[27] W. D. M. Rae, A. C. Merchant, and J. Zhang, Phys. Lett. B **321**, 1 (1994).
[28] J. Zhang and W. D. M. Rae, Mod. Phys. Lett. A **9**, 599 (1994).
[29] P. Tikkanen, J. Keinonen, and A. Kangasmki, Phys. Rev. C **47**, 145 (1993).
[30] G. S. Anagnostatos, Phys. Rev. C **51**, 152 (1995).
[31] G. S. Anagnostatos, Phys. Rev. C (to be published).
[32] J. Leech, Math. Gaz **41**, 81 (1957).
[33] G. S. Anagnostatos, Lett. Nuovo Cimento **22**, 507 (1978).
[34] G. S. Anagnostatos, Lett. Nuovo Cimento **28**, 573 (1980).
[35] G. S. Anagnostatos, Lett. Nuovo Cimento **29**, 188 (1980).
[36] G. S. Anagnostatos, J. Yapitzakis, and A. Kyritsis, Lett. Nuovo Cimento **32**, 332 (1981).
[37] G. S. Anagnostatos and C. N. Panos, Phys. Rev. C **26**, 260 (1982).
[38] C. N. Panos and G. S. Anagnostatos, J. Phys. G **8**, 1651 (1982).
[39] G. S. Anagnostatos and C. N. Panos, Lett. Nuovo Cimento **41**, 409 (1984).
[40] W. F. Hornyak, *Nuclear Structure* (Academic, New York, 1975).
[41] C. W. de Jager, H. de Vries, and C. de Vries, At. Data Nucl. Data Tables **14**, 479 (1974).
[42] P. H. Stelson and L. Grodzins, Nucl. Data, Sec. A **1**, 21 (1965).
[43] E. Merzbacher, *Quantum Mechanics* (Wiley, New York, 1975).
[44] G. H. Fuller and V. W. Cohen, Nucl. Data, Sec. A **5**, 433 (1969).
[45] M. M. Hindi, J. H. Thomas, D. C. Radford, and P. D. Parker, Phys. Rev. C **27**, 2902 (1983).
[46] W. E. Hunt, M. K. Mehta, and R. H. Davis, Phys. Rev. **160**, 782 (1967).

[47] M. K. Mehta, W. E. Hunt, and R. H. Davis, Phys. Rev. **160**, 791 (1967).
[48] G. T. Gaskey, Ph. D. thesis, University of Wisconsin, 1983, available from University Microfilms, Ann Arbor, Michigan.
[49] S. J. Sanders, L. M. Martz, and P. D. Parker, Phys. Rev. C **20**, 1743 (1979).
[50] J. H. Billen, Phys. Rev. C **20**, 1648 (1979).
[51] S. R. Riedhauser, Ph.D. thesis, University of Wisconsin, 1983, available from University Microfilms, Ann Arbor, Michigan.
[52] Y. Fujiwara, Prog. Theor. Phys. **62**, 122 (1979).
[53] F. Nemoto and H. Bandō, Prog. Theor. Phys. **47**, 1210 (1972).
[54] Y. Fujiwara, H. Horiuchi, and R. Tamaga, Prog. Theor. Phys. **61**, 1629 (1979).
[55] M. V. Zhukov, Sov. J. Nucl. Phys. **40**, 568 (1984).
[56] M. Harvey, *Adv. Nucl. Phys.*, edited by M. Baranger and E. Vogt (Plenum, New York, 1968), Vol. 1, and quotations therein.
[57] H. Feldmeier and P. Manakos, Z. Phys. A **281**, 379 (1977).
[58] M. K. Benerjee, C. A. Levinson, and G. J. Stephenson, Jr., Phys. Rev. **178**, 1709 (1969).
[59] H. Rebel, G. W. Schweimer, J. Specht, G. Schatz, R. Lähken, D. Habs, G. Hauser, and H. Klewe-Nebenius, Phys. Rev. Lett. **26**, 1190 (1971).
[60] S. Marcos, H. Flocard, and P. H. Heenen, Nucl. Phys. A **410**, 125 (1983).
[61] F. Nemoto and H. Bandō, Prog. Theor. Phys. **47**, 1210 (1972).
[62] F. Nemoto, Y. Yamamoto, H. Horiuchi, Y. Suzuki, and K. Ikeda, Prog. Theor. Phys. **54**, 104 (1975).
[63] A. H. Wapstra and N. B. Gove, Nucl. Data Tables **9**, 267 (1971).
[64] R. H. Spear, Phys. Rep. **73**, 369 (1981).
[65] J. Zofka and G. Ripka, Nucl. Phys. A **168**, 65 (1971).
[66] W. Y. Ng and L. E. H. Trainor, Can. J. Phys. **52**, 541 (1974).